IEEE Access
Multidisciplinary | Rapid Review | Open Access Journal

Received February 15, 2020, accepted February 24, 2020, date of publication March 3, 2020, date of current version March 13, 2020.

Digital Object Identifier 10.1109/ACCESS.2020.2977962

Detection of Ovarian Tumors in Obstetric Ultrasound Imaging Using Logistic Regression Classifier With an Advanced Machine Learning Approach

ZHENG ZHANG AND YIBO HAN
School of Software, Nanyang Institute of Technology, Nanyang 473000, China
Corresponding author: Zheng Zhang (zhangzheng@nyist.edu.cn)

This work was supported by the 2019 Cross Science Research Project of Nanyang Institute of Technology, Research on Intelligent Mining and Recommendation of Zhang Zhongjing Prescription Based on Deep Neural Network, under Grant 201913502.

ABSTRACT This paper addresses the use in different stages of pregnancy of ultrasound imaging and to examine the tumors diagnosed during lactation or pregnancy. There are recent advancements in the application of obstetric ultrasound and imaging techniques helpful for improving the outcome of the pregnancy using various Learning techniques. This paper addresses the need to implement sustainable ultrasound standards with an acceptably high maternal and perinatal mortality rates to provide better and more affordable, quality Ultrasonic Flaw (UT) equipment which can improve Obstetric health care. The state-of-the-art learning approach for obstetric ultrasound is a category of methods in machine learning that are gaining popularity and attracting interest in various fields, including image processing and computer vision. In this paper advanced Machine learning processes map a raw input image to the desired output image using logistic regression classifier(LRC) and Convolution neural networks (CNNs) are of particular interest among all Machine learning methods. Furthermore, we have utilized the Internet of Medical Things (IoMT) for obstetric tumor image segmentation and identification of tumors for the medical experts. The experimental results show the LRC based on CNN can be utilized to predict the output of the ultrasound of obstetric with increased maternal and perinatal mobility rates.

INDEX TERMS Machine learning, convolution neural network, logistic regression model, obstetric ultrasound, IoMT.

I. BACKGROUND AND INTRODUCTION

Presently, Ultrasound (US) imaging is a safe, noninvasive diagnostic method for internal organ diagnosis. The ultrasound image is more portable and prevalent, compared with other imaging tools, such as Magnetic Resonance image (MRI), computerized tomography (CT), etc., [1]. It helps in the assessment and management of medical conditions, diagnosing the causes of infection, pain, and swelling of internal organs. Ultrasound imaging has become a general prenatal check-up tool [2]. The fetal abdominal circumference, biparietal size, head circumference, humerus length, femur and the duration of the crown-rump, are used to analyze and calculate biometric fetus parameters [3]. To estimate gestational size, age, and weight, monitor growth and detect fetal abnormalities, the circumference of the head (HC) is measured [4].

Ultrasound imaging is the most common technique for monitoring fetal diagnostic factors in obstetrical settings [5]. Fetal biometric measurements are useful to predict the intrauterine growth constraints and fetal fetus maturity as well as to estimate the gestational age (i.e. fetal biparietal diameter estimates (BPD), head circumferences (HC) and abdominal circumferences (AC) [6]. For diagnosis, the organ images are analyzed by an obstetrician and gynecologist using various effective techniques. When a sufficient sound wave beam is sent through a transducer in the human body, the ultrasound image is molded. Appropriate ultrasound images are produced by replication from internal organisms [7]. Besides, due to their properties, the sprocket, attenuation,

The associate editor coordinating the review of this manuscript and approving it for publication was Wei Wei.

missing borders, and artifacts could influence them, making the segmentation task more complicated [8].

Pregnancy scanning and fetal development remained primitive and its applications in the field of obstetric imaging increased dramatically as sonographic technology progressed [9]. The ultrasound today provides a detailed image of the fetus, placenta, uterus, cervix, and adnexa as well as the dynamic visualization of the heart of the fetus, fetal motion, and fetal patterns of breathing with the actual two-or three-dimensional (3D) scans and spectral and Doppler color sonography [10]. While the photographs of the pregnant patient or otherwise used, none provides the safety [11], flexibility [12], and clarity that the ultrasound provides [13], [14]. Recently, the Machine Learning Convolutional Neural Networks(ML-CNN) have been an important choice for various image processing activities, including detection [15], classification [16], registration, and segmentation. ML-CNNs have been a strong choice for Fetal ultrasound research and the Machine learning workflow in obstetric image processing has been shown in Figure.1.

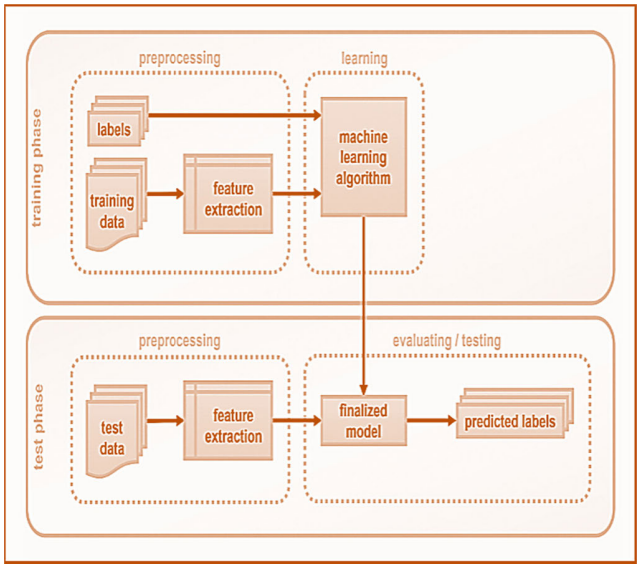

FIGURE 1. Machine learning workflow.

In this study, the cause-specific survival of pregnant or lactating women diagnosed with malignant as well as those women pregnant with the post-cancer disease test data in the preprocessing stage of the training phase has been analyzed. The report results for the most common malignancies in premenopausal women, namely cervical, breast, thyroid and ovarian cancers [16], malignant lymphoma [17], malignant melanoma [18], leukemia and brain tumors in the test phase with testing and evaluation. Besides, to allow accurate detection and treatment during pregnancy in maternal tumors. The Internet of Medical Things (IoMT) and its recent developments include a new dimension to the improvement and creation of an intelligent system in the medical industry [19]. However, due to growing peripherals in inpatient care, the medical data of IoMT systems are constantly increasing in the present scenario.

Based on the study the main involvement of this paper as follows as,

- A Machine Learning-based Convolutional Neural Network (ML-CNN) framework for an obstetric image collection is molded and trained in the training phase.
- The learned features are used for a highly efficient obstetric imaging system, which works for a large multi-modal data set collection which has been analyzed in the test phase.
- The logistics regression algorithm has been proposed for the high-level feature and fine-tunes the whole model with testing and evaluation.

The remainder of the paper as follows in section 1 and section 2 discussed the background study of the research. In section 3 the modeled ML-CNN for extracting the image with LRC has been mathematically analyzed. In section 4 the experimental results with numerical outcomes. Finally, section 5 concludes the research paper.

II. LITERATURE SURVEY

Kim *et al.* [20] proposed the ML-based Automatic identification of fetal abdominal circumference (AIFAC) from images of ultrasound. This paper introduced a method for the automatic estimation of fetal Biometry from 2D ultrasound data through multiple processes consisting of a specially designed neural convolution (CNN) and a U-Net network for each process. These techniques of machine learning take into account the decisions of clinicians, anatomical structures, and the characteristics of ultrasound images. Finally, clinical data validate the effectiveness of the AIFAC approach. The AIFAC method of Machine learning is a hierarchical system that imitates the abdominal circumstances calculation technique of a clinician procedure.

Kirk *et al.* [21] introduced the pregnancies of unknown location (PUL) approaches to identify the model in an early clinical environment of pregnancy. A logistic regression model was previously developed to predict where the PULs become ectopic. The chorionic gonadotropin (hCG) based on the human model is a logistic regression model. The hormonal information was entered into the model that was available in the Microsoft Excel kit on the clinic computer and for each case, the predicted outcomes were reported according to this model. The template was calculated against the cost of failed PULs and intrauterine pregnancies to detect an ectopic pregnancy.

Brattain *et al.* [22] suggested the machine learning approach (MLA) for ultrasound medical and clinical workflow. The ultrasound is the ability to create a video in real-time key strength. The advantages of spatiotemporal data have been widely used to improve results by machine learning method which is applied to echocardiography and obstetrics. Machine learning is an especially powerful method to extract nonlinear characteristics of the information. This is especially promising in ultrasound, which typically has no

simple or hand-designed predictable acoustic patterns. The machine learning-based smart diagnostic assistant framework for learning multiscale and multimodal observations over the period is converted into the aggregated machine intelligence will be able to observe, lead the end-user, assess new data and assist with decision making in medical sustainable quantitative models. This system is likely not only the overall result of treatment to improve the clinical workflow significantly.

Huang *et al.* [23] introduced the Ultrasound Computer-aided diagnosis (US-CAD) utilizing Machine learning for fetal ultrasound standard plane detection. One category of fetal ultrasound, a standard plane is the fetal facial standard. The clinical data can evaluate the biparietal diameter of the fetus from the fetal facial standard plane and detect the malformation. The efficient features will increase precision and reduce the computational complexity. The collection of data is not consistent with ultrasound CAD systems. The selection of features affects the quality of the final diagnosis in the conventional ultrasonic CAD System. The Traditional ultrasound system CAD's common feature can be separated into four types: descriptor features, textural, morphological, and model-based.

Salehi *et al.* [24] suggested the voxel wise fully convolutional network (VFCN) for Fetal MRI automatic brain extraction using Machine learning. They have developed and assessed an architecture of a voxel-wise network using a 3-way system, the post processing based on the algorithm of the linked components and a morphological closing procedure as the final step. They have used completely convolutional layers rather than fully connected layers to accelerate testing. To ensure that the whole image is tested in a network of convolutional layers, while voxels are tested in a network of fully connected layers.

To overcome these issues, a method of Machine learning consisting of multiple CNNs (ML-CNN) and a U-Net that are intended to achieve many goals such as an initial estimate, manipulation of many ultrasound objects such as spinning and acoustic shadowing, spinal location identification, semantic segmentation of ripe regions, and acceptance for a proper identification of ovarian tumors. The proposed method is beneficial over the previous CNN-based approaches with a relatively low amount of data due to the combination of several CNNs and a U-Net. The main benefit of IoMT sensors for healthcare is to reduce the time between assessment, identification, and treatment.

III. OBSTETRIC ULTRASOUND IMAGE SEGMENTATION USING MACHINE LEARNING-BASED CONVOLUTIONAL NEURAL NETWORKS (ML-CNN) METHOD

In this paper, a Machine Learning-based Convolutional Neural Network model for obstetric image ultrasound to detect ovarian tumors during pregnancy. The activations from previous layers have been converted in convolutional layers with a set of small filters, often of size 3×3, in a tensor S(j, i) where j the layer number and i is filter number. By sharing the same weights with each filter across the entire input domain, that is translation equivalence with each layer, the number of weights that have to be learned can be reduced considerably. The explanation for this weight-sharing is the fact that features in one part of the picture are possibly present in other pieces. If you have a filter that can detect horizontal lines, you can use it to detect wherever it occurs. in this research, the datasets have been taken from stanford.edu/datasets.

A nonlinear active function provides feature maps of a convolutional layer. This allows nearly every nonlinear function to be approximate for the entire neural network. In general the activation functions are extremely simple, straight-linear units or ReLUs stated as ReLU(y) = max(0,y), or variants such as leaky ReLUs or variable ReLUs. The functional maps are fed to new tensors utilizing activation functions. Each functionality map generated by feeding a data layer or more is typically pooled into a pooling layer. Pooling actions take input in small grid areas and generate individual numbers for every field. Typically, the number is determined using zero or the mean function. As the input image changes little in the activation maps, the pooling layers give the convolutional neural network some translation invariance. Figure 2 shows the basic building blocks of the proposed ML-CNN system.

CNN has been used to detect the dark area of the polar ultrasound image transformed. To obtain the initial abdominal circumstances estimation, we applied the Hough transform to the semantically segmented image. From the conventional neural network, we gathered labeled training data $\{(y_l, x_l)\,|l = 1, \ldots M\}$ from fetal ultrasound images, where y_l Refers to 128×128, the target pixel centered patch and $x_l = (x_{l1}, \ldots x_{l4}) \in \Re^4$ Indicates the target pixel class.

The objective of this CNN is to develop the function f^*, which is capable of classifying an input patch y into four classes. The labeled training data enable this feature to be measured,

$$f^* = argmin_f \sum_{l=1}^{M} \|f\,(y_l) - x_l\| \tag{1}$$

Then, the minimization problem (1) in determining f^* is equivalent to the definition of satisfying parameters θ^*,

$$\theta^* = argmin_\theta \frac{1}{M} \sum_{l=1}^{M} K(y_l, x_l; \theta) \tag{2}$$

As shown in equation (2) where the cross-entropy loss function K is to calculate the error between the true label x and inferred output $q_j(y; \theta)$ for every class:

$$K\,(y_l, x_l; \theta) = -\sum_{j=0}^{M} x_l log q_j(y_l; \theta) \tag{3}$$

We have calculated the minimization problem for batch training.

In this research, the datasets have been taken from stanford.edu/datasets which has been shown in Figure.3. The optimal treatment for ovarian cancer phase involves salpingo-oophorectomy dual, para-aortic lymphadenectomy, and total hysterectomy as well as omentectomy. The key surgeries for the diagnosis included unilateral salpingo-oophorectomy, ovarian cystectomy only, USO plus multiple biopsies, or more extreme USO, pelvic and paraaortic

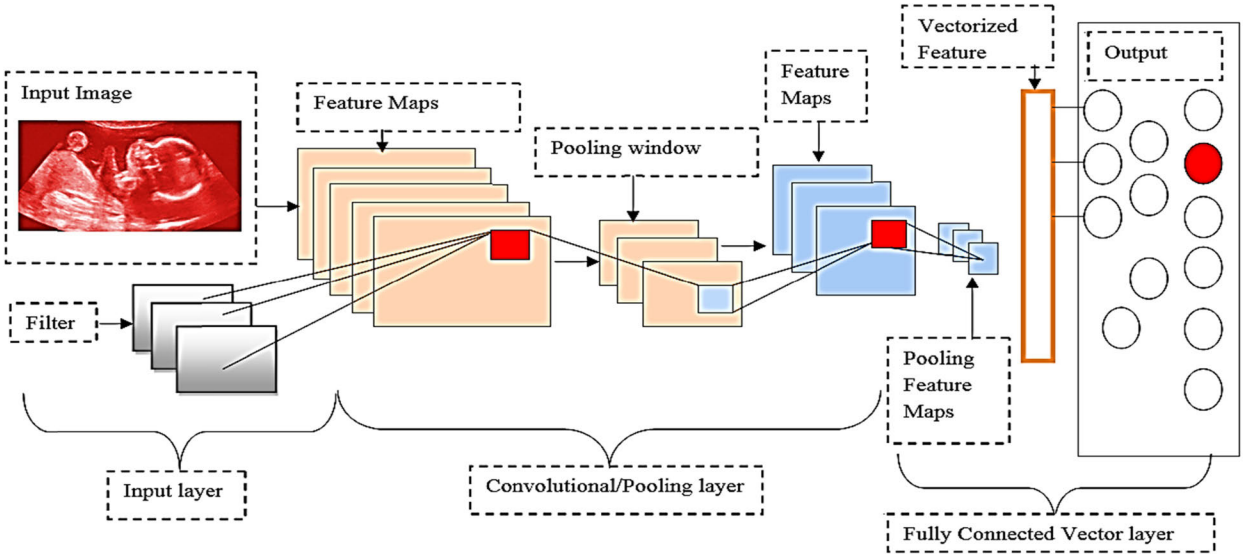

FIGURE 2. ML-CNN system with Logistic vectorized analysis.

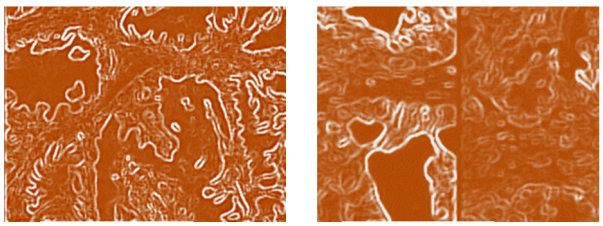

(a). Tumor Free abdominal wall (b). Tumor abdominal wall

FIGURE 3. primary ovarian tumor histopathologic appearances.

lymphadenectomy, peritoneal biopsies, infrasonic omentectomy, appendectomy, and even lymphatic and paraaortic lymphadenectomy. Figure.3(a) shows the anterior abdominal wall and abdominal organs have been tumor-free. Figure.3 (b) shows the Tumor abdominal wall with Histopathology revealed mucinous cystadenocarcinoma (intestinal type) of the right ovary. Antineoplastic chemotherapy is used to prevent newly inserted tumors or residual ovarian cancer cell growth to continue the pregnancy. Each anti-neoplastic agent is cytotoxic theoretically. A key concern is the trans placental transfer of the agent to the fetus has been classified using feature map case analysis which has been discussed below.

A. MATHEMATICAL CASE ANALYSIS: 1-FEATURE CLASSIFICATION

For classification, CNN with a logistic regression model is applied based on high-level features. The data for high-level classification and extraction of features will be given below. First, feature maps are generated from the spectral feature with the offset η, the initial spectral vector is split into τ simple spectral. The spectral vector can be expressed,

$$a_j = u(w), \quad 1 \le j \le \eta, \tau(j-1)+1 \le w \le \tau(j-1)+s \tag{4}$$

As shown in equation (4) where u is the original spectral vector, a_j is the jth spectral vector with the length s. To obtain a spectral feature map, we have set the independent variable two basic spectral vectors. The feature map is then given,

$$N_l = sqrt\left(a_j a_j^T\right), \quad 1 \le j,\ i \le \eta, 1 \le l \le m \tag{5}$$

As shown in equation (5) where m is the number of feature maps and N_l is the l^{th} spectral feature map and received n^{th} spectral vector to spectral feature maps the spectral input data as the ML-CNN inputs based on the computation using the logistic regression model.

B. MATHEMATICAL CASE ANALYSIS:2-LOGISTIC REGRESSION MODEL AND ML-CNN TRAINING

As inferred from the algorithm.1. ML-CNNs have two types of layers: the convolution layer and the down sampling layer. The forward propagation of the CNN layer can be defined as,

$$b_i^k = f\left(\sum_{j\in P} b_j^{k-1} * l_{ji}^k + a_i^k\right) \tag{6}$$

As shown in equation (6) where f is the sigmoid function, P denotes an input maps election, b_i^k Indicates the feature map activation value output I in layer k, l_{ji}^k is the bias linked with feature map output i in layer k, l_{ji}^k is the kernel connection feature map input j in layer k-1 to feature map output i in layer k. $*$ denotes the convolution multiplication.

The down-sample layer forward propagation can be computed as,

$$b_i^k = f\left(\delta_i^k down\left(b_i^{k-1}\right) + a_i^k\right) \tag{7}$$

As shown in equation (7) were down denotes a subsampling function. Usually, this function is summed up the output feature map over every single patch so that in both spatial dimensions the output feature map is y times smaller.

Algorithm 1 Single Modality Classification

Input: j, i, l
Output: f^*, a_j, b_i^k, Q
#Preprocessing
For (i=0)
$$f^* = argmin_f \sum_{l=1}^{M} \|f(y_l) - x_l\|$$
For (j=0)
$$K(y_l, x_l; \theta) = -\sum_{j=0}^{M} x_l log q_j(y_l; \theta)$$
#Feature Map
For (i=1)
$$a_j = u(w), 1 \le j \le \eta, \tau(j-1)+1 \le w \le \tau(j-1)+s$$
For (j=1)
$$b_i^k = f\left(\delta_i^k down\left(b_i^{k-1}\right) + a_i^k\right)$$
#Segmentation
If (l=0)
$$\beta_i^k = \delta_i^{k+1}\left(f'(v_i^k) \circ up\left(\beta_i^{k+1}\right)\right)$$
Else
$$Q(X = j|U, S, a) = w(SU + a) = \frac{e^{S_j U + a_j}}{\sum_i e^{S_j U + a_i}}$$
End if
End for
End for
End for
End for
End
Return

Output feature map i in layer k is multiplicative by δ_i^k. a_i^k is the output bias map i in layer k.

To evaluate the sensitivities of CNN layers, the up sampling and sensitivity map down sampling layers are used, Further, it has been multiplying it with the activation derivative map at layer k element-wise. It can be expressed as,

$$\beta_i^k = \delta_i^{k+1}\left(f'\left(v_i^k\right) \circ up\left(\beta_i^{k+1}\right)\right) \tag{8}$$

As shown in equation (8) where β_i^k is the feature map sensitivity value i in CNN layer k, ∘ indicates the element-wise multiplication, β_i^k Indicates the inputs to map total weighted sum myself in layer k and Up (.) indicates an Up-sampling function.

Now that the sensitivities of the convolution layer are present, the gradients can be determined as follows for bias and kernel weights based on the corollary computation.

Corollary 1:

$$\frac{\partial G}{\partial a_i} = \sum_{v,u} (\beta_i^k)_{vu} \tag{9}$$

$$\frac{\partial G}{\partial l_{ji}^k} = \sum_{v,u} \left(\beta_i^k\right)_{vu} (q_j^{k-1})_{vu} \tag{10}$$

As shown in the above equation where (v,u) is the coordinate in the convolution map, E is the squared error, b_i^k and q_j^{k-1} is the patch in layer b_i^{k-1} Which is multiplied element-wise by using l_{ji}^k during forwarding propagation to assess the element at the coordinate (v,u) in the output CNN map b_i^k.

The use of full convolution with the convolution layer kernel and multiply it with the activating derivative layer map at layer k element-wise to calculate the sensitivities of the down sampling layer.

$$\beta_i^k = f'\left(v_i^k\right) \circ \left(\Delta_i^{k+1} * l_{ji}^{k+1}\right) \tag{11}$$

As shown in equation (12) where Δ_i^{k+1} is the increasing sensitivity map in the Downsampling Layer with the input feature map with the weak positive stain as shown in Figure.4(a). The additive bias can be measured using Equation (9). The sensitivities of the down sampling layer have been identified. The multiple bias δ included the original down-sampled map calculated during forwarding propagation in the current layer.

$$r_i^k = down\left(b_i^{k-1}\right) \tag{12}$$

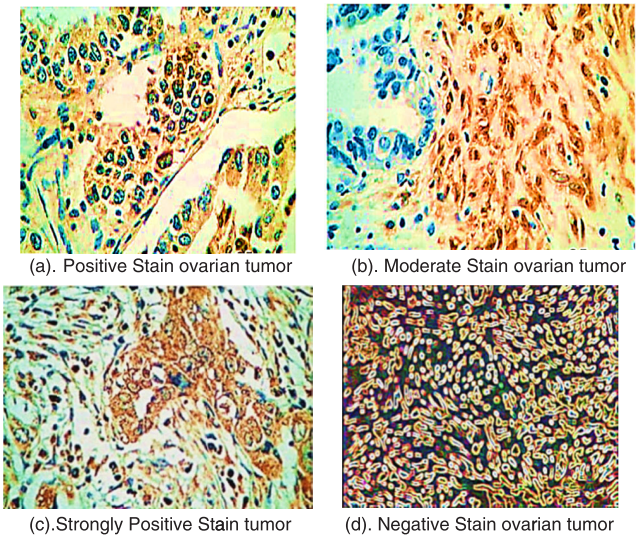
(a). Positive Stain ovarian tumor
(b). Moderate Stain ovarian tumor
(c).Strongly Positive Stain tumor
(d). Negative Stain ovarian tumor

FIGURE 4. Stains of the ovarian samples.

The gradient is then given to the multiplication bias.

$$\frac{\partial G}{\partial \delta_i} = \sum_{v,u} (\beta_i^k \circ r_i^k)_{vu} \tag{13}$$

The utilized different samples are taken from stanford.edu/ datasets. Figure 4 (a) shows the samples of ovarian tumors with a stain indicator are weakly positively stained. Figure 4(b) shows Ovarian samples with a marked staining index are moderately positive. Figure 4 (c) Samples of ovarian tumors with marked staining index have strongly positive. Figure 4(d) shows the Normal ovarian samples with marked staining index are negative or weakly positive.

The logistic regression model is added to the top of the functional extraction layers to form a CNN. To finalize the entire model, the backward propagation algorithm is utilized. The classification of logistic regression applies to Multi-classification soft-max regression tasks to analyze the moderate positive value as shown in Figure.4.(b). The input U

function is flattened by the ML-CNN's output features, thus the likelihood of the input feature of class j,

$$Q(X = j\,|U, S, a) = w\,(SU + a) = \frac{e^{S_j U + a_j}}{\sum_i e^{S_j U + a_i}} \quad (14)$$

As shown in equation (14) where X is the classification result, S is the weight and a is the bias, S_j and a_j indicate the bias connecting and weight the output unit j, and w is the softmax function. The output layer unit number is the total class number which helps to identify the strong positive value of the stains as shown in Figure.4(c). The ML-CNN's-LR classification is built into a Machine learning system. The labels created by most ML-CNN / LR classifiers will then be labeled as each pixel. The input layer is the same dimension as the last ML-CNN layer is used to detect the negative stain as shown in Figure.4(d).

C. MATHEMATICAL CASE ANALYSIS: 3: CLASSIFICATION PERFORMANCE

In this paper, the Machine learning-based convolutional neural network (ML-CNN) method for the detection and diagnosis of the ovarian tumor during pregnancy. The single modality classification algorithm has been proposed for the neural network feature extraction of the obstetric image with ultrasound technology. A typical CNN consists of two components: an extractor for a feature and a classifier. The extractor function is used for sorting input pictures on ''feature maps,'' which represent different object features. The characteristics may include corners, lines, circular arches, etc., which are relatively invariant to position distortions or shifting. The function extractor may, for example, be made up of several optional sub-sampling and convolutional layers. The proposed algorithm achieves high accuracy of an obstetric tumor image. Here the input layers are of elements that are connected to the convolutional in order to shape the parameters of the input layer and with filter assistance, it is transferred to the pooling layer for the purpose of reducing the sizes of the elements and identification of tumors. Then the maximum value is taken and connected to the convolutional layer to remove the filters.

Here all the input numbers of data are collected in the form of n and that is determined as the maximum length of the Logic regression model with input function y. The error data are collected in the form of data and it is calculated to form a reference value for each segment to analyze the tumor. The reference equation is determined as

$$B_{ref} = \frac{(y_{n-1} - y_0)}{n} \quad (15)$$

Here the sum of values of the above equation is determined as

$$\text{Sum Y} = \sum_{j=0}^{n-1} y_j \quad (16)$$

The above equation which can be written in the form of logistic manner as

$$\text{Surprise Y} = \sum_{j=0}^{n-1} Y_j^2 \quad (17)$$

When the above equation is calculated in the form of step format and the equation can be denoted as

$$\text{Step Y} = \sum_{j=0}^{n-1} j y_j \quad (18)$$

Here the entire modules end with the initial phase components and it transfers all the input parameters in B_{ref} and each and every value of the first segment is denoted as y_{ref} and the initial point is denoted as p_0 and termed as a node point for the identification of tumors.

In the proposed model the entire learning algorithm is formulated and integrated with the IoMT platform. Here $y = \{y_1, y_2, y_3, \ldots..., y_k\}$. And the polynomial function of the equation is denoted as follows in the Corollary metric:3

Algorithm 2 Logistic Classification Learning Algorithm

Input
Output
Begin
If(K=1)
$\boldsymbol{g\,(K) = \sum_{j=0}^{t} b_j(k_j - k_0) + e\,(k_0) + \epsilon;}$
$\boldsymbol{x_{ij} = x_{ij} - \alpha \frac{\delta p(Q,a)}{\delta x_{ij}}}$
$\boldsymbol{a_{ij} = x_{ij} - \alpha \frac{\delta p(Q,a)}{\delta x_{ij}}}$
else
$\boldsymbol{g_0(k_m) = g\,(k_m)}$
$\boldsymbol{g_1(k_m) = g_{q-1}(k_m) - g_{q-1}(k_{m-1})}$
End if
End begin

As inferred From the algorithm.2. The activation parameters a_{ij} are denoted with a number of different parameters and that weighed with a various coefficient $(\boldsymbol{b_j}, \boldsymbol{k_j - k_0})$ and the values for the normal function distribution are determined in $\boldsymbol{g\,(K)}$. Here the constant coefficients are determined as b_j and e as a stream of functions. ϵ denotes as standard normal distribution $(\frac{\delta p(Q,a)}{\delta x_{ij}})$ of the normal value as denoted as $\boldsymbol{x_{ij}}, \boldsymbol{a_{ij}}$. The points are denoted as $k_1 - k_0 = k_j - k_{j-1}$ for j = 1, 2…n this is equated in above algorithm.2 for tumor analysis. Therefore $b_j(k_j - k_0) = B_{ref}$ then the corresponding data model equation can be represented as an estimated model and behavior stream model. From the algorithm.2. the m^{th} model of input is simplified as

$$g(k_m) = B_{ref} + \epsilon \quad (19)$$

In the above equation, the prediction analysis model is expressed as m+1 that is chosen from the stream data points and g (K) that can be an approximately denoted as

$$g_t(k_{m+1}) \approx B_{ref} \quad (20)$$

Therefore, in the above equation, the qth factor is calculated as

$$g_q(k_{m+1}) \approx g_{q-1}(k_{m+1}) + g_{q-1}(k_m) \quad (21)$$

Here the restricted values and the intermediate points are expressed in the data stream points. Thus the proposed models are denoted with various sampling rates of the equation. Here again, the predicted tumor value can be determined as follows:

$$B_q = H[g_q(k_m)]; \tag{22}$$

Here H [.] denotes the average value of the function, here the problem will be raised when placing the random values that are expressed in the total sensor values that possess negative effects.

The negative effects are determined as the variance function of the threshold value θ. Thus the independent random noise standard deviation is expressed as follows

$$\mathrm{VAR}(\sum_{j=1}^{n}(g_1(k_{m-j+1})) = \sqrt{n}(\mathrm{VAR}(g_q(k_m))) = \sqrt{n}\sigma. \tag{23}$$

And finally, the estimated value is determined as follows

$$B_q = \mathrm{H}[\frac{\sum_{j=1}^{n} g_q(k_{m-j+1})}{n}] \tag{24}$$

Here the error of estimation is denoted as $\frac{\sigma}{\sqrt{n}}$. Thus the independent random noise standard deviation is derived.

In terms of average precision (AP), the average recall (AR), accuracy and the measurement of F1 the performance of the proposed classification task framework is measured based on corollary metrics.

Corollary2:

$$AP = \frac{1}{M}\sum_{j=1}^{M}\frac{TP_j}{TP_j + FP_j} \tag{25}$$

$$AR = \frac{1}{M}\sum_{j=1}^{M}\frac{TP_j}{TP_j + TN_j} \tag{26}$$

$$Accuracy\ (ACC) = \frac{1}{M}\sum_{j=1}^{M}\frac{TP_j + TN_j}{TP_j + TN_j + FP_j + FN_j} \tag{27}$$

$$F1\ Score = 2 \times \frac{AP \times AR}{AP + AR'} \tag{28}$$

As shown in the above equation where, TP is truly positive and refers to the number of images of class l and properly classified (FP is the wrong positive) and the number of images of class l, TN is true negative and indicates the number of images correctly categorized as non-class l, FN is false negative and denotes images of class l but not classified or 'M' denotes the total number of class where TP is truly positive and indicates the number of frames of class l. The proposed ML-CNN with a logistic regression classifier achieves a better classification accuracy of the ovarian tumor images than previous hyperspectral classification methods.

IV. NUMERICAL ANALYSIS AND VALIDATION

Machine learning becomes even more important by constantly improving technological features for accurate and multidimensional IoMT data to improve diagnostic accuracy. Overall, the inclusion of Machine education in IoMT can offer radical innovations in medical image processing, disease diagnostics, analytics of medical big data and breakthrough medical applications. Here the image database analysis has been shown in Figure 5 shows the classification analysis based on the IoMT platform using the logistic learning model. The accurate measurements of different ultrasound signs, including sensitivity, specificities and likelihood ratios are measured. A meta-analysis was carried out with more than three studies recording the ultrasound sign and datasets of 12 images taken for analysis have been shown below in Figure.6. Precision estimates for the individual studies with estimated sensitivity and distinction, Further the accuracy between ectopic and intrauterine pregnancies has been analyzed. The proposed ML-CNN method achieves a high specificity ratio when compared to other existing methods.

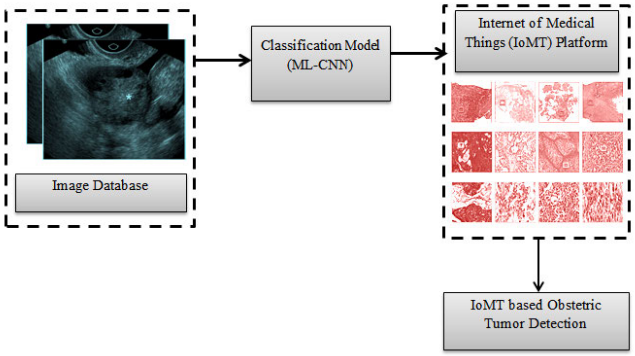

FIGURE 5. Obstetric tumor detection using machine learning technique on IoMT platform.

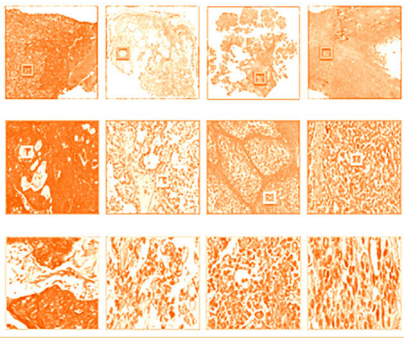

FIGURE 6. Datasets of 12 images taken for analysis from the pathological information database.

Figure. 6. shows the test samples of partitioned images from the main dataset, the trained neural network can be tested. The test data were not in any way used in the practice and therefore provide the network with ''out-of-sample'' data. This offers an evaluation of the network's performance with real-world data.

Historical or medical risk factors that may show an increased likelihood of fetal abnormality should be carefully tested for the obstetric population. The methodical and complete screening ultrasound test should include the examination of each of several recommended scan plane views

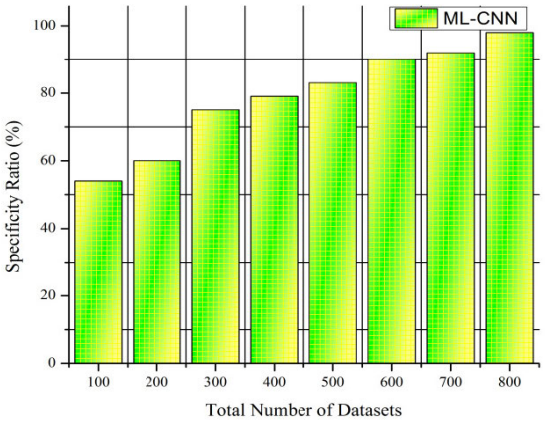

(a) Specificity Ratio

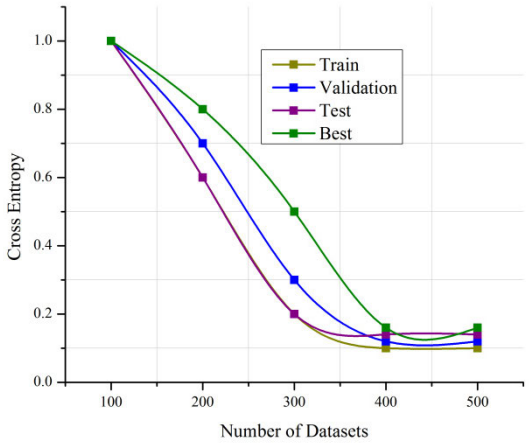

(b) Cross-Entropy

FIGURE 7. Specificity Vs cross-entropy.

to optimize the sensitivity of diagnosis with a high specificity ratio as shown in Figure.7(a). Further, to show that a standard healthcare service was provided, the completion and methodical examination should be closely documented with descriptive text and image documents. Here as shown in Figure.7(b) the original spectral vector, a_j is the jth spectral vector with the length s. To obtain a spectral feature map, the set of independent variables two basic spectral vectors for validation and test. In addition, as shown in Figure.8. the performance ratio of the proposed ML-CNN method. To ensure diagnosis accuracy as well as increasing the need for repeat scans by insufficient testing, it is important to improve the performance and consistency of ultrasound screening. The design and implementation of quality assurance protocols are a way to improve the testing, leading in the course to higher visualization levels of the ovaries among recorded clinics.

As inferred from the equation (6) where f is the sigmoid function, P denotes an input map selection, b_i^k Indicates the feature map activation value output I in layer k, l_{ji}^k is the bias linked with feature map output i in layer k, l_{ji}^k is the kernel connection feature map input j in layer k-1 to feature map output i in layer k. $*$ denotes the convolution multiplication with a high sensitivity ratio as shown in Figure.9.

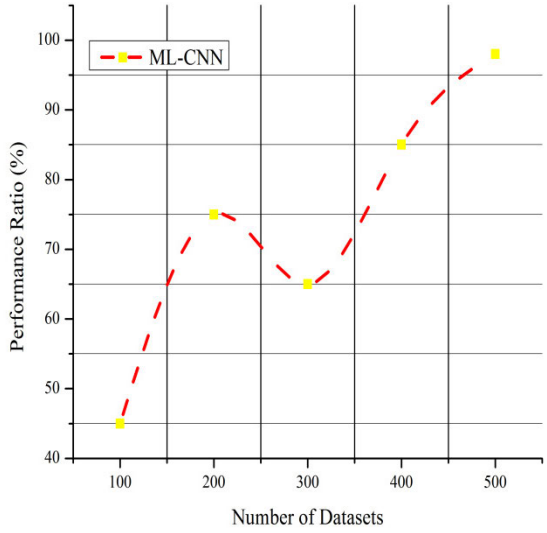

FIGURE 8. Performance ratio.

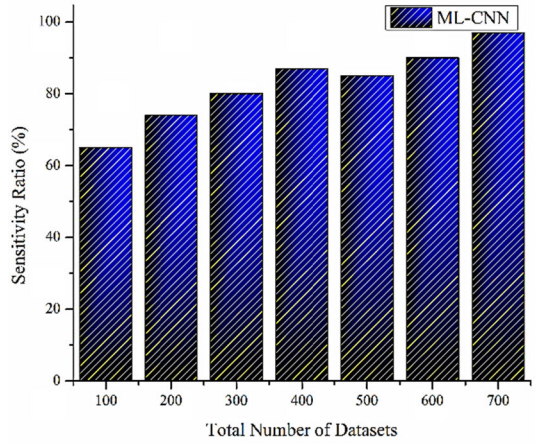

FIGURE 9. Sensitivity ratio.

Feature depictions have been used for the recovery of medical objects in all three fully linked layers of the training model. The performance of the retrieval results has been evaluated using both methods, i.e. with and without the predicted class label. For class prediction, the improvement in performance in terms of precision is evident. Figure 10 shows the precision ratio of the proposed ML-CNN method. The precision ratio is high when compared to other existing methods.

Table 1 shows the precision ratio of the proposed system. The precision ratio and accuracy ratio are ways to explain the error between the two image values. Figure 8 displays the precision plots for representation features extracted with class prediction and without class prediction.

In this paper, two parameters for comparison have been used, one classification accuracy, average accuracy and mean classification alert and the other mean average precision [25]. The precision-recall curve is a pixel dependent calculation using an uncertainty matrix for the evaluation of the

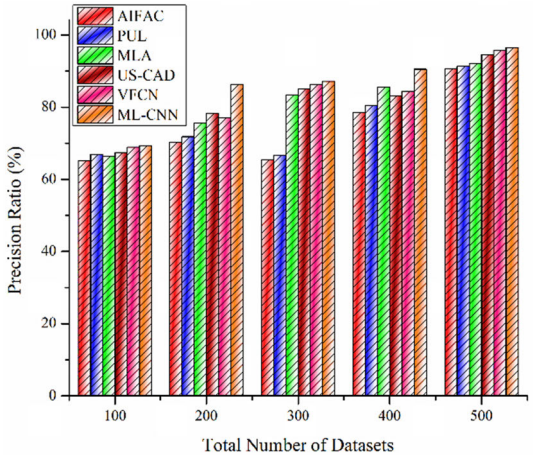

FIGURE 10. Precision ratio.

TABLE 1. Precision ratio.

Total Number of Datasets	AIFAC	PUL	MLA	US-CAD	VFCN	ML-CNN
100	65.1	66.9	66.4	67.4	68.9	69.3
200	70.3	71.8	75.5	78.3	77.1	86.2
300	65.4	66.7	83.3	85.1	86.3	87.1
400	78.5	80.5	85.5	83.2	84.4	90.5
500	90.6	91.3	92.1	94.5	95.8	96.5

performance [26] of the algorithm. Precision informs about the validity of the segmentation results and recalls the correctly identified pixels on the edges of an image. Higher precision and reminder value mean that the segmentation method shows good results.

Table 2 shows the recall ratio of the proposed ML-CNN method. The segmentation approach is accomplished when the alert quality is small and when the value of precision is higher over-segmentation is achieved. The percentage of true positive pixels sensitivity or true positive values or recall (figure 11).

TABLE 2. Recall ratio.

Total Number of Datasets	AIFAC	PUL	MLA	US-CAD	VFCN	ML-CNN
100	45.1	46.5	47.6	48.9	49.4	50.3
200	52.2	56.6	66.9	69.3	59.4	70.4
300	76.4	73.3	77.4	80.6	83.6	87.4
400	70.5	84.4	86.5	89.2	72.5	87.6
500	80.6	89.9	83.1	87.4	92.2	99.1

In this paper, the growth chart showing the fetal weight as compared with the gestational age. The calculated from a combination of measured and predictive error ratios of 10-20%. Abdominal circumference measurement is the measurement of fetal growth which is most useful, representing a fetal subcutaneous fat volume and liver length,

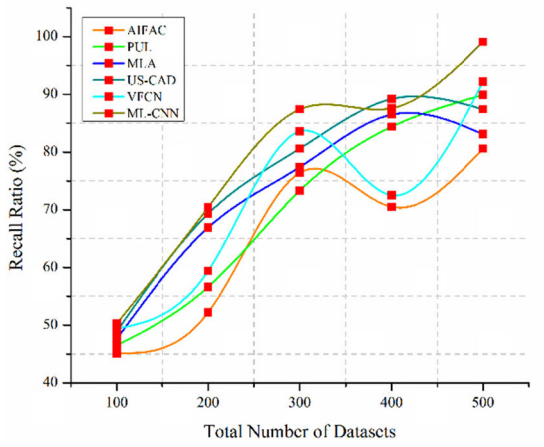

FIGURE 11. Recall ratio.

which are in turn correlated with fetal nutrition. The proposed ML-CNN method has less error rate in terms of image segmentation when compared to other existing methods. Figure 12 shows the Error Rate analysis of the proposed system.

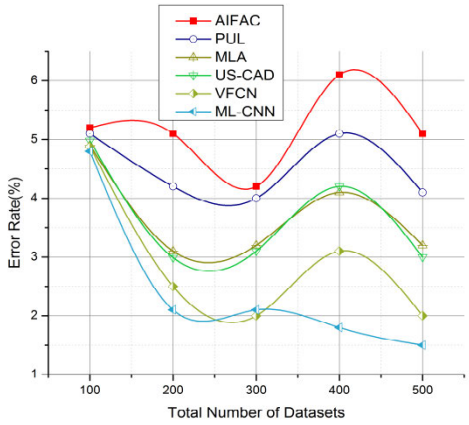

FIGURE 12. Error rate.

The experimental results show the logistic regression classifier (LRC) based on CNN can be utilized to predict the output of the ultrasound of obstetric with increased maternal and perinatal mobility rates. Here the entire modules end with the initial phase components and it transfers all the input parameters where each and every value of the first segment analysed for the identification of tumor in an effective manner.

V. CONCLUSION

This paper presents Machine learning framework for the detection of ovarian tumor images from content by training for the classification task in a Machine learning-based convolutional neural network. We used a logistic regression classifier for the feature map, segmentation, and classification. Furthermore, a Single modality classification algorithm has been proposed. Fortunately, the ultrasound is a non-invasive

and effective instrument, which can help diagnose most of these problems, avoid the consequences of these complications and direct care in some cases. In obstetrics, therefore, broader use of ultrasound is encouraged. It is important to train every obstetric doctor and sister-in-law in basic ultrasound use in obstetrical care. A Machine model was used directly to classify obstetric images with the inclusion of traditional image features. The ML-CNN-LR classifiers extract the obstetric tumor image with a high classification of accuracy. The precision and recall have been used to test the performance of the proposed ML-CNN for obstetric image retrieval.

REFERENCES

[1] M. Nagayama, Y. Watanabe, A. Okumura, Y. Amoh, S. Nakashita, and Y. Dodo, "Fast MR imaging in obstetrics," *RadioGraphics*, vol. 22, no. 3, pp. 563–580, May 2002.
[2] C. B. Benson and P. M. Doubilet, "The history of imaging in obstetrics," *Radiology*, vol. 273, no. 2S, pp. S92–S110, Nov. 2014.
[3] B. P. Harrison and C. S. Crystal, "Imaging modalities in obstetrics and gynecology," *Emergency Med. Clinics*, vol. 21, no. 3, pp. 711–735, 2003.
[4] H. Chen, D. Ni, J. Qin, S. Li, X. Yang, T. Wang, and P. A. Heng, "Standard plane localization in fetal ultrasound via domain transferred deep neural networks," *IEEE J. Biomed. Health Informat.*, vol. 19, no. 5, pp. 1627–1636, Sep. 2015.
[5] H. Chen, Q. Dou, D. Ni, J. Z. Cheng, J. Qin, S. Li, and P. A. Heng, "Automatic fetal ultrasound standard plane detection using knowledge transferred recurrent neural networks," in *Proc. Int. Conf. Med. Image Comput. Comput.-Assist. Intervent.* Cham, Switzerland: Springer, Oct. 2015, pp. 507–514.
[6] Y. Gao, M. A. Maraci, and J. A. Noble, "Describing ultrasound video content using deep convolutional neural networks," in *Proc. IEEE 13th Int. Symp. Biomed. Imag. (ISBI)*, Apr. 2016, pp. 787–790.
[7] P. M. Shakeel, T. E. E. Tobely, H. Al-Feel, G. Manogaran, and S. Baskar, "Neural network based brain tumor detection using wireless infrared imaging sensor," *IEEE Access*, vol. 7, pp. 5577–5588, 2019, doi:10.1109/access.2018.2883957.
[8] T. L. A. van den Heuvel, H. Petros, S. Santini, C. L. de Korte, and B. van Ginneken, "Automated fetal head detection and circumference estimation from free-hand ultrasound sweeps using deep learning in resource-limited countries," *Ultrasound Med. Biol.*, vol. 45, no. 3, pp. 773–785, Mar. 2019.
[9] L. Wu, J.-Z. Cheng, S. Li, B. Lei, T. Wang, and D. Ni, "FUIQA: Fetal ultrasound image quality assessment with deep convolutional networks," *IEEE Trans. Cybern.*, vol. 47, no. 5, pp. 1336–1349, May 2017.
[10] A. S. Becker, M. Mueller, E. Stoffel, M. Marcon, S. Ghafoor, and A. Boss, "Classification of breast cancer from ultrasound imaging using a generic deep learning analysis software: A pilot study," *Brit. J. Radiol.*, vol. 91, no. 1083, Dec. 2017, Art. no. 20170576.
[11] P. Gomathi, S. Baskar, P. M. Shakeel, and V. R. S. Dhulipala, "Identifying brain abnormalities from electroencephalogram using evolutionary gravitational neocognitron neural network," *Multimedia Tools Appl.*, Feb. 2019, doi: 10.1007/s11042-019-7301-5.
[12] Z. Sobhaninia, S. Rafiei, A. Emami, N. Karimi, K. Najarian, S. Samavi, and S. M. R. Soroushmehr, "Fetal ultrasound image segmentation for measuring biometric parameters using multi-task deep learning," in *Proc. 41st Annu. Int. Conf. IEEE Eng. Med. Biol. Soc. (EMBC)*, Jul. 2019, pp. 6545–6548.
[13] J. C. A. Carvalho, "Ultrasound-facilitated epidurals and spinals in obstetrics," *Anesthesiol. Clinics*, vol. 26, no. 1, pp. 145–158, Mar. 2008.
[14] M. Yaqub, B. Kelly, A. T. Papageorghiou, and J. A. Noble, "A deep learning solution for automatic fetal neurosonographic diagnostic plane verification using clinical standard constraints," *Ultrasound Med. Biol.*, vol. 43, no. 12, pp. 2925–2933, Dec. 2017.
[15] H. Chen, Y. Zheng, J. H. Park, P. A. Heng, and S. K. Zhou, "Iterative multi-domain regularized deep learning for anatomical structure detection and segmentation from ultrasound images," in *Proc. Int. Conf. Med. Image Comput. Comput.-Assist. Intervent.* Cham, Switzerland: Springer, Oct. 2016, pp. 487–495.
[16] F. Liu, H. Jang, R. Kijowski, T. Bradshaw, and A. B. McMillan, "Deep learning MR imaging–based attenuation correction for PET/MR imaging," *Radiology*, vol. 286, no. 2, pp. 676–684, 2017.
[17] A. Wójtowicz, P. Żywica, K. Szarzyński, R. Moszyński, S. Szubert, K. Dyczkowski, and M. Wygralak, "Dealing with uncertainty in ovarian tumor diagnosis," in *Modern Approaches in Fuzzy Sets, Intuitionistic Fuzzy Sets, Generalized Nets and Related Topics*, vol. 2. 2014, pp. 151–158.
[18] J. Kaijser, T. Bourne, L. Valentin, A. Sayasneh, C. Van Holsbeke, I. Vergote, A. C. Testa, D. Franchi, B. Van Calster, and D. Timmerman, "Improving strategies for diagnosing ovarian cancer: A summary of the international ovarian tumor analysis (IOTA) studies," *Ultrasound Obstetrics Gynecol.*, vol. 41, no. 1, pp. 9–20, Dec. 2012.
[19] L. P. Shulman, "Preoperative sonographic features of borderline ovarian tumors," *Yearbook Obstetrics, Gynecol. Women's Health*, vol. 2006, pp. 300–302, Jan. 2006.
[20] B. Kim, K. C. Kim, Y. Park, J.-Y. Kwon, J. Jang, and J. K. Seo, "Machine-learning-based automatic identification of fetal abdominal circumference from ultrasound images," *Physiol. Meas.*, vol. 39, no. 10, Oct. 2018, Art. no. 105007.
[21] E. Kirk, G. Condous, Z. Haider, C. Lu, S. Van Huffel, D. Timmerman, and T. Bourne, "The practical application of a mathematical model to predict the outcome of pregnancies of unknown location," *Ultrasound Obstetrics Gynecol.*, vol. 27, no. 3, pp. 311–315, Feb. 2006.
[22] L. J. Brattain, B. A. Telfer, M. Dhyani, J. R. Grajo, and A. E. Samir, "Machine learning for medical ultrasound: Status, methods, and future opportunities," *Abdominal Radiol.*, vol. 43, no. 4, pp. 786–799, Feb. 2018.
[23] Q. Huang, F. Zhang, and X. Li, "Machine learning in ultrasound computer-aided diagnostic systems: A survey," *BioMed Res. Int.*, vol. 2018, pp. 1–10, Mar. 2018.
[24] S. S. M. Salehi, S. R. Hashemi, C. Velasco-Annis, A. Ouaalam, J. A. Estroff, D. Erdogmus, S. K. Warfield, and A. Gholipour, "Real-time automatic fetal brain extraction in fetal MRI by deep learning," in *Proc. IEEE 15th Int. Symp. Biomed. Imag. (ISBI)*, Apr. 2018, pp. 720–724.
[25] P. Looney, G. N. Stevenson, K. H. Nicolaides, W. Plasencia, M. Molloholli, S. Natsis, and S. L. Collins, "Automatic 3D ultrasound segmentation of the first trimester placenta using deep learning," in *Proc. IEEE 14th Int. Symp. Biomed. Imag. (ISBI)*, Apr. 2017, pp. 279–282.
[26] J. J. Cerrolaza, M. Sinclair, Y. Li, A. Gomez, E. Ferrante, J. Matthew, C. Gupta, C. L. Knight, and D. Rueckert, "Deep learning with ultrasound physics for fetal skull segmentation," in *Proc. IEEE 15th Int. Symp. Biomed. Imag. (ISBI)*, Apr. 2018, pp. 564–567.

ZHENG ZHANG graduated from the Nanjing University of Technology, in 2015. He is currently working with the School of Software, Nanyang Technological University. His research interests include machine learning cloud computing and big data.

YIBO HAN graduated from the China University of Geosciences (Beijing), in 2015. He is currently working with the School of Software, Nanyang Technological University. His research interests include the Internet of Things, muti-access edge computing, analysis of big data.